Express Polymer Letters Vol.16, No.6 (2022) 665–676
Available online at www.expresspolymlett.com
https://doi.org/10.3144/expresspolymlett.2022.48

Research article

Highly spectrally selective dual-layer cellulose-based composite material for daytime radiative cooling

Xitao Yang[1], *Haoqun Hong*[1,3], *Haiyan Zhang*[1,3], *Xiaobin Hong*[2*]

[1]School of Materials and Energy, Guangdong University of Technology, 510006 Guangzhou, China
[2]School of Mechanical and Automotive Engineering, South China University of Technology, 510640 Guangzhou, China
[3]Guangdong Sunlite Science & Technology Co., No. 9, Erheng Road, Small and Medium Enterprise Park, Zhangpeng Village, Mayong Town, 523145 Dongguan, China

Received 15 November 2021; accepted in revised form 8 March 2022

Abstract. Passive radiative cooling is a key technology to solve the global warming and energy waste caused by refrigeration. However, because of the high price and complex manufacturing process, the application of daytime radiative cooling materials in the field of building materials is hindered. Here, we studied a low-cost radiative cooling cellulose-based composite material prepared from wood powder that exhibits highly selective infrared emission and high solar reflectivity. And we use the evaporation deposition technique to form a dual-layer structure with silica microspheres in the lower layer. The radiative cooling film based on the intrinsic absorption of lignocellulose and silica microspheres exhibits not only high infrared emissivity of 98.7% in the 'atmospheric window' range but also exhibits high reflectivity of 98.44% in the visible light range. We have also found that the performance of the radiative cooling film is the best when the content of silica microspheres reaches 30 wt%, and the film exhibits a cooling of 9.6 °C under direct sunlight. The preparation method of low-cost and high-performance radiative cooling material provided in this article is expected to provide a reference for the application of radiative cooling materials in building materials.

Keywords: *polymer composites, biocomposites, polymer membranes, daytime radiative cooling, silica microsphere*

1. Introduction

For a long time, researchers have been committed to the development of advanced infrared adaptive materials. Materials that use infrared characteristics for camouflage and radiative cooling have become current research hotspots [1]. Radiative cooling is a key technology to solve the global warming caused by the greenhouse effect and energy waste generated by refrigeration which is currently a major energy consumption part [2]. Cellulose contains functional groups (such as C–O, C–O–H, and C=O), which cause the infrared intrinsic absorption of cellulose through molecular vibration, so the cellulose is considered to have great potential as a radiative cooling material [3, 4]. At the same time, cellulose is a widely sourced, degradable, and environmentally friendly material [5]. Since 1908, when natural cellulose composites were used as biological composites, cellulose-based composites have been developed and applied [6]. Cellulose is widely used in the fields of biomimetic materials [7], biomedicine [8, 9], and ultraviolet shielding [10, 11], because of its wide sources and easy chemical modification. Therefore, extracting cellulose from natural materials and using it as a radiative cooler not only have a great significance to the realization of an environmentally friendly functional material, but also provide a reference for the application of radiative materials in building materials.

The essence of thermal radiation is the energy transfer of the energy level transition of the object [12].

*Corresponding author, e-mail: scut_hongxiaobin@126.com

Objects with different temperatures will exchange heat by means of thermal radiation [13]. Therefore, radiative cooling materials use the means of radiation to transmit heat through the atmosphere to the cosmic black body (Temperature is assumed to be 3 K) to achieve the effect of passive cooling. This cooling method not only conforms to the energy transfer rules but also creates a green and environmentally friendly cooling method. Therefore, radiative cooling materials are widely used to reduce the cooling load of buildings [12, 14] and mitigate urban heat island effect [15, 16] in a spontaneous and recyclable way. However, the application of radiative cooling materials in building materials still has problems such as high costs and complex production processes [17]. Simultaneously, buildings usually require daytime cooling, and the daytime radiative cooling materials not only need to have the high infrared emissivity in the 'atmospheric window' (8–13 μm) range, but also need to have the high reflectivity and the low absorption in the solar radiation wavelength range. Such problems have made the radiative cooling materials limited in the field of building materials [17, 18]. At present, the daytime radiative cooler is mainly realized by designing an excellent daytime radiative cooling structure, and the daytime radiative cooling structure is composed of high reflectivity in the solar spectral range and high emissivity in the 'atmospheric window' range [19]. Among them, the daytime radiative cooling structure is mainly divided into the multilayer planar photonic structure, which has a high reflectivity in the solar radiation range by alternately stacking high and low refractive index material layers and is used for obtaining high emissivity in the 'atmospheric window' range by making the use of material resonance and designing a specific number of layers [2, 20, 21], the metamaterials and two-dimensional or three-dimensional photonic structures which require complex and expensive micro-manufactured [22, 23], the radiative cooling polymers doped with nanomaterial resonators [24, 25], and the radiative cooling materials provided in the form of simple and easy-to-use coatings [26–28]. The complex structure of daytime radiative cooling hinders the application of radiative cooling materials, and cellulose-based composite materials suitable for daytime radiative cooler are still rarely reported [4, 29].

In this work, we use wood flour as raw material to prepare a cellulose-based composite material that can be used for daytime radiative cooling. The preparation method is simple, and the price is low. The average thickness of the films is 142 μm; if the yield of lignocellulose is about 56.67%, excluding energy consumption and labor, the cost of preparing a 1 m^2 radiative cooling film is about $246, but the cost of raw materials is only 6 cents. It is expected to provide ideas for the application of radiative cooling materials in the construction industry. The material proposed in the article uses the characteristics of easy chemical modification of cellulose to be compounded with silica microspheres and achieves an average emissivity as high as 98.7% in the 'atmospheric window' range through the intrinsic absorption of lignocellulose and silica microspheres [4]. At the same time, we also explored the influence of silica microsphere content on the material properties, and we found that when the silica microsphere content is 20 wt%, the average reflectivity to the visible light range is as high as 99.71%, and the addition of silica microspheres has almost no effect at the top of the radiative cooling film; however, the infrared emissivity at the bottom of the film will increase significantly at the 9.7 μm wavelength range. When the final silica content is 30 wt%, the radiative cooling performance of the film is the highest. Finally, we built a radiative cooling performance test device to demonstrate the daytime radiative cooling performance of cellulose-based composites.

2. Experimental

2.1. Sample preparation

The solution of 0.4 mol/l Na_2SO_3 (97%, Tianjin Damao Chemical Reagent Factory, China) and 4 mol/l NaOH (96%, Tianjin Zhiyuan Chemical Reagent Co., Ltd, China) were prepared in proportion, and wood powder (40 mesh, eucalyptus, Weihua Perfume Factory, China) was dried and weighted for use. First, the wood powder was mixed and reacted in a closed environment at 100 °C for 10 hours to remove lignin. Then the reaction product was added into a solution prepared by a certain proportion of sodium chlorite (80%, Shanghai Maclean Biochemical Technology Co. Ltd., China), deionized water, and glacial acetic acid (99.5%, Tianjin Zhiyuan Chemical Reagent Co. Ltd., China) after washing and filtering. The mixture was reacted for 5 hours in a closed environment at 70 °C for bleaching, and this process is repeated 1–2 times. After the delignified and bleached lignocellulose was washed and dried, we weighed 1 g of the sample, and dispersed it in

25 ml of glacial acetic acid, and stirred for 30 min, then the mixture was added with 0.144 g of concentrated sulfuric acid (95–98%, Guangzhou Chemical Reagent Factory, China) and 9 ml of glacial acetic acid and stirred for 30 minutes to perform pretreatment. When the sample was evenly dispersed in the solution, the solid was dissolved in 32 ml of acetic anhydride (98.5%, Guangzhou Chemical Reagent Factory, China), stirred for 30 minutes, and left for 16 hours for acetylation modification. After standing the sample solution, the mixture was added with 10 ml glacial acetic acid, 10 ml deionized water, and 1.35 g concentrated sulfuric acid to hydrolyze at 80 °C for 10 minutes to reduce the degree of acetylation of lignocellulose, and finally, we added deionized water to stop the reaction and dried the sample after filtering and washing. The absolute ethanol (99.7%, Tianjin Zhiyuan Chemical Reagent Co. Ltd., China) as the solvent, the ammonia (25%, Tianjin Zhiyuan Chemical Reagent Co. Ltd., China) as the catalyst, and the ethyl orthosilicate (38%, Tianjin Zhiyuan Chemical Reagent Co. Ltd., China) was hydrolyzed and prepared silica microspheres at a stirring speed of 400 rpm at room temperature. Then we washed and dried with absolute ethanol and deionized water in turn to obtain pure silica microspheres. Finally, the sample was dissolved in a 10:1 (volume ratio) mixed solution of acetone and water, and silica microspheres were added to prepare a radiative cooling film with a particle content of 0, 10, 20, and 30 wt% (weight percentage). At room temperature (25 °C), we placed the solution in a fume hood to evaporate. The evaporation process took 48 hours. The high temperature will lead to a too fast evaporation rate and results in cracking. Low temperature will lead to too slow evaporation rate, and the porous structure will be difficult to form. The evaporation environment should be dry because the sample wet will also cause the film to crack.

2.2. Sample characterization

The top and bottom of the sample film were observed by using a field emission scanning electron microscope (SEM, SU8010, Hitachi Ltd., Japan) and a tungsten filament scanning electron microscope (S-3400N-II, Hitachi Ltd., Japan) at working voltages of 15 and 5 kV to study their morphology and structure. In order to characterize the high reflection characteristics of the sample film to sunlight and the high infrared emission characteristics in the atmospheric window, we use the UV-3600 Plus UV-VIS-NIR spectrophotometer (UV-3600 Plus, Shimadzu Ltd., Japan), including the 60 mm solid integrating sphere (ISR-603) accessory. Then we measured the absorption and reflectance of the sample film in the wavelength range of 360–2000 nm. The Nicolet 6700 Fourier Transform Infrared Spectrometer (Nicolet 6700, Nicolet Ltd., America) was added to the integrating sphere accessory, and the sample film was installed between the gold mirror and the metal plate, and the sample's reflectivity in the mid-infrared wavelength range of 2.5–15.5 μm was measured with a resolution of 8 cm^{-1}. And we used formula conversion to determine the absorptance and infrared emissivity of the sample film in the mid-infrared wavelength range of 7–14 μm. In order to further verify the distribution of the sample film particles, we performed X-ray diffraction spectroscopy (XRD) on the surface of each sample film and determined the composition and distribution of the sample film through phase analysis. Finally, we built a radiative cooling performance test device using a polystyrene foam box, a thermal sensor, and a temperature recorder. The radiative cooling performance of the sample film was tested by the radiative cooling performance test device during sunny days. The schematic diagram and physical diagram of the test device are shown in Figure 1.

3. Results and discussion

Figure 2 shows the microstructure of samples with different silica content. From top to bottom are the SEM pictures of the film with 0, 10, 20, and 30 wt% silica content. The pictures in the left column (Figure 2a, 2c, 2e, 2g) are the micrograph of the top of the film, and the pictures in the right column (Figure 2b, 2d, 2f, 2h) are the micrograph of the bottom of the film. The top of the film is surrounded by the intricate acetylated lignocellulose microfibrils, and the microfibrils form a porous structure. Because the volatilization rate of acetone molecules in the acetone solution system during the solvent volatilization process is much greater than the volatilization rate of water molecules, the volatilization of acetone and the insoluble acetyl lignocellulose in water will cause the precipitation of acetyl lignocellulose and the coalescence of the polymer-rich phase. When the acetone is completely volatilized, the microfibrils of lignocellulose precipitate out of the solution and coexist with water molecules to form a structure in

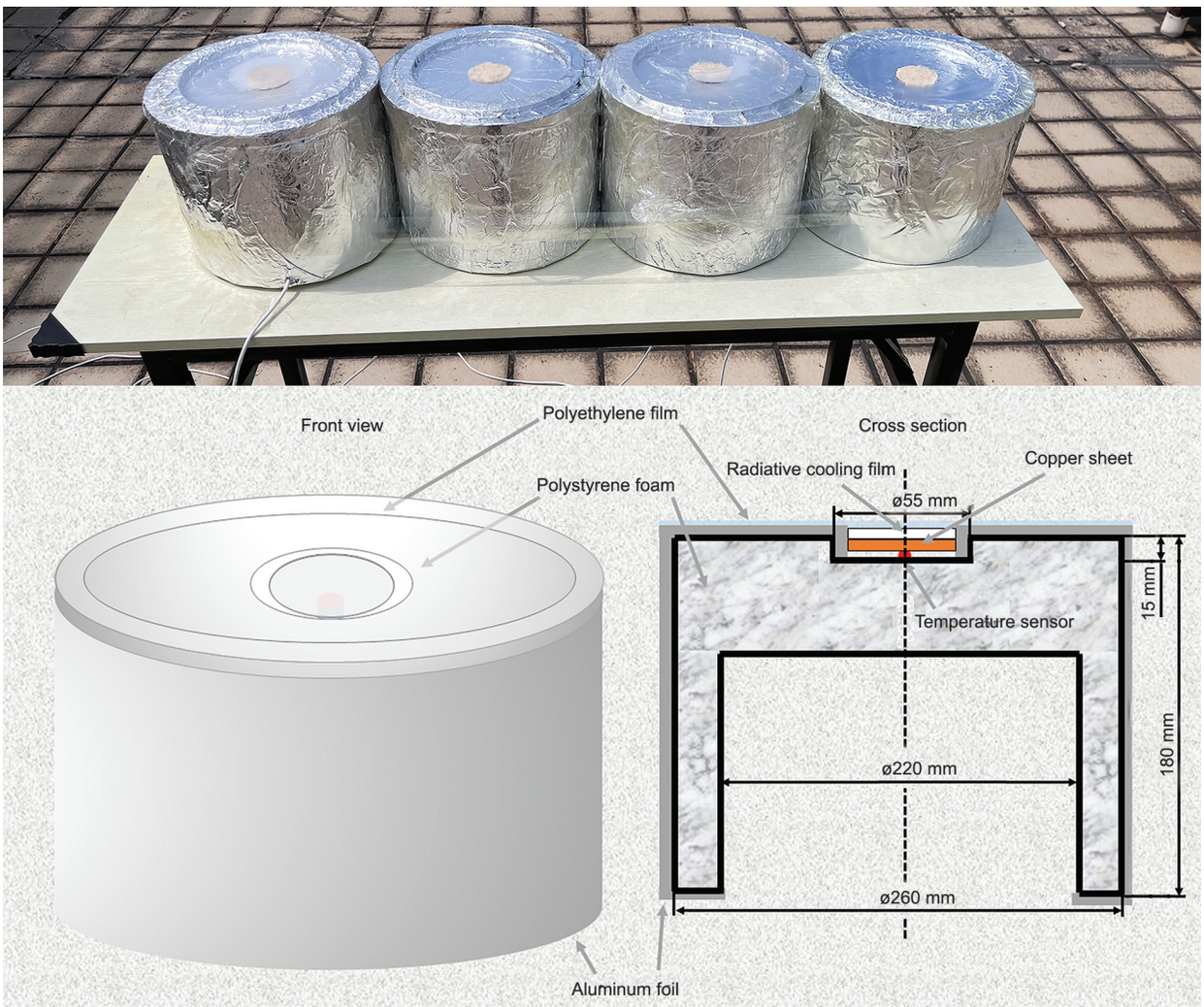

Figure 1. The schematic diagram of the radiative cooling performance test device.

which water molecules are wrapped by acetylated lignocellulose microfibrils. As the water molecules evaporate, the structure of the acetylated lignocellulose microfibrils remains, and it forms a porous structure [30].

From the comparison of Figure 2a, 2c, 2e, 2g and Figure 2b, 2d, 2f, 2h it is found that the silica microspheres all appear at the bottom of the sample film. During the evaporation of the solvent, the silica microspheres will sink to the bottom due to gravity, which causes the silica microspheres to accumulate on the bottom of the radiative cooling film. In addition, comparing Figure 2a, 2c, 2e, 2g and Figure 2b, 2d, 2f, 2h, it is found that the film has denser acetylated lignocellulose at the bottom. During the volatilization of the acetone molecule, the acetylated lignocellulose part precipitates, and the acetylated lignocellulose part precipitating was deposited due to gravity, resulting in dense cellulose microfibrils at the bottom of the film [30]. From the above results, it can be seen that the reaction process of the whole experiment is shown in Figure 3. After preparing acetyl lignocellulose and silica microspheres, firstly, the acetylated lignocellulose is dissolved in the acetone solution, and the silica microspheres are dispersed in the solution. Subsequently, due to the successive volatilization of acetone and water, the acetylated lignocellulose precipitated, and the polymer-rich phase coalesced. This can be seen from the uneven thickness of the acetylated lignocellulose microfibrils. Then, during the volatilization process, the silica microspheres and the partially precipitated microfibrils of acetylated lignocellulose are deposited together, the lower layer of radiative cooling film forms a structure where the silica microspheres are wrapped by the microfibrils, and the upper layer of radiative cooling film forms a porous structure due to the influence of water molecules.

Since the realization of daytime radiative cooling material has a decisive relationship with the solar

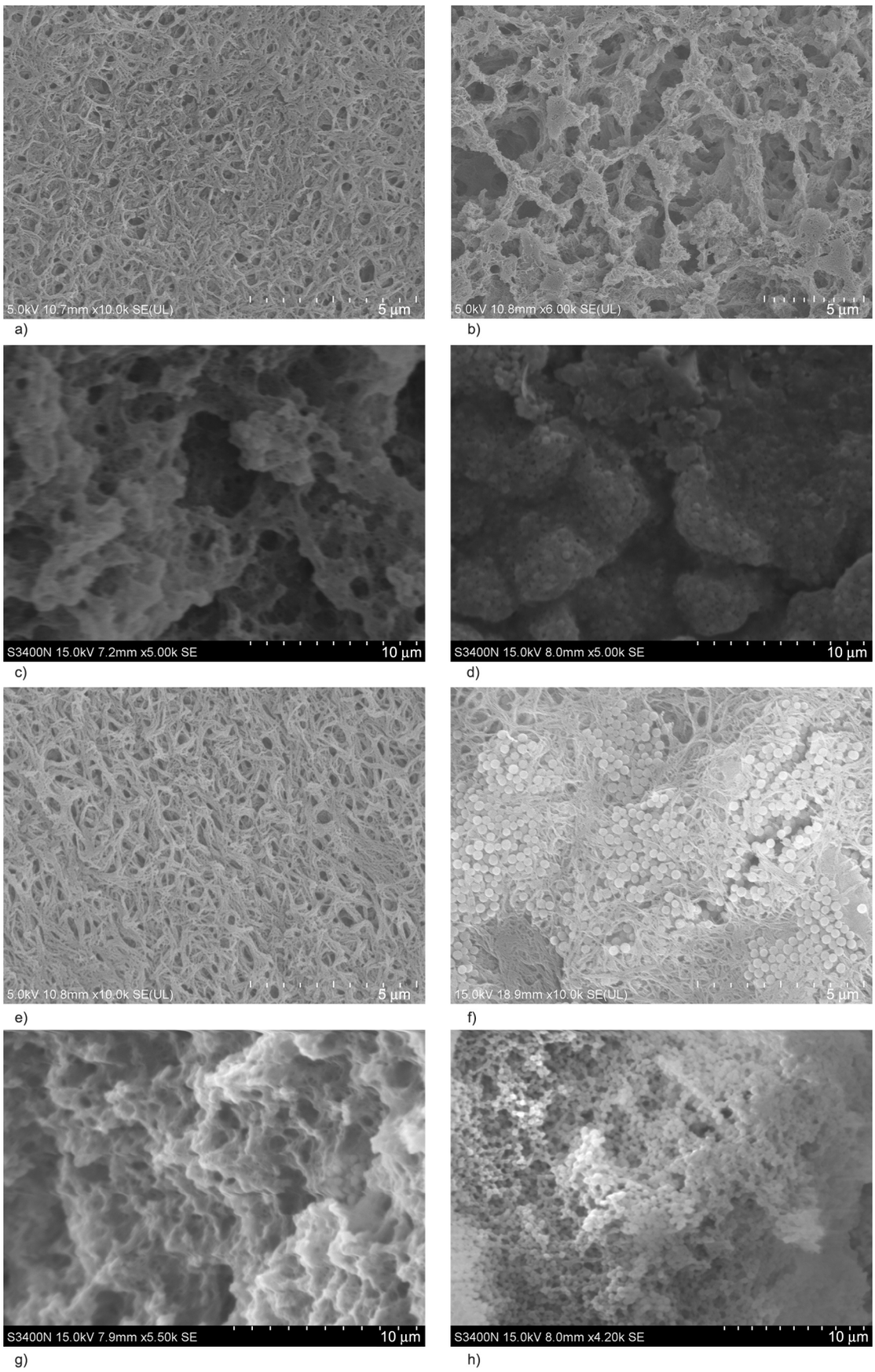

Figure 2. The SEM images of left (left column, a, c, e, g) and right (right column, b, d, f, h) sides of the radiative cooling film with 0, 10, 20, and 30 wt% silica microspheres content. The diameter of the silica microspheres is about 0.24 μm. Among them, the scale of a, b, e, f is 5 μm, and the scale of c, d, g, h is 10 μm.

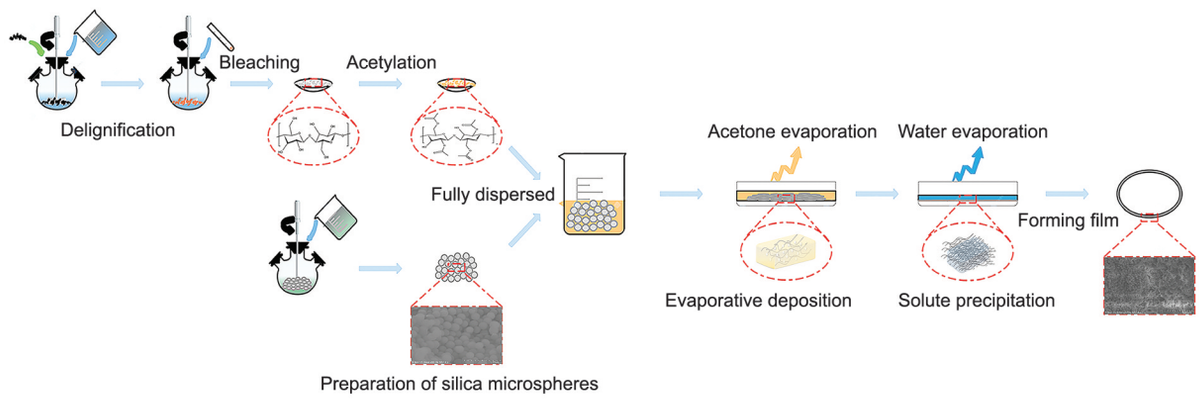

Figure 3. Flow chart and principle diagram of the preparation of the radiative cooling film.

radiation range absorbance and reflectance of the material surface, we use UV-3600 Plus UV-VIS-NIR spectrophotometer with an integrating sphere accessory to directly measure the absorbance and the reflectivity of the sample film. Figure 4 hows the sample film's reflectivity and absorbance with 0,10, 20, 30 and 40 wt% content of silica microspheres in the 360–2000 nm wavelength range. The results show that the sample film generally has low absorption of light in the 360–2000 nm range, and the average absorbance are respectively 0.172, 0.038, 0.025, 0.017 and 0.254, the reflection of light in the range of 360–2000 nm is generally higher, and the average reflectance are respectively 76.65, 90.95, 86.48, 87.05 and 61.37%. Then we quoted the data of direct normal spectral irradiance [W/(m^2·nm)] obtained after the National Renewable Energy Laboratory (NREL) modeled the American Society for Testing and Materials (ASTM) G-173 solar irradiance spectrum, and we normalized it as the solar spectrum of AM (atmospheric mass) 1.5 mid-latitude countries (such as China) is used to analyze the absorption and reflection of solar radiation energy by the radiative cooling film. We can find that the addition of silica microspheres can significantly increase the reflectivity of the film and the radiative cooling film with a silica microsphere content of 20 and 30 wt% has a reflectivity in the 360–2000 nm wavelength range almost exceeding the normalized solar irradiance, while the absorbance in the 360–1100 nm wavelength range is much less than the normalized solar irradiance. However, when the content of silica microspheres in the film exceeds 10 wt%, the addition in silica content will increase the absorbance and decrease the reflectivity of the film in the wavelength range of 1100–2000 nm. The most obvious is the 1900 nm wavelength range, which is caused by the absorption of silica in the near-infrared band [31]. We also found that when the content of silica microspheres exceeds 20 wt%, the reflectivity of the film in the wavelength range of 360–1100 nm decreases to varying degrees with the increase of silica microsphere content. The

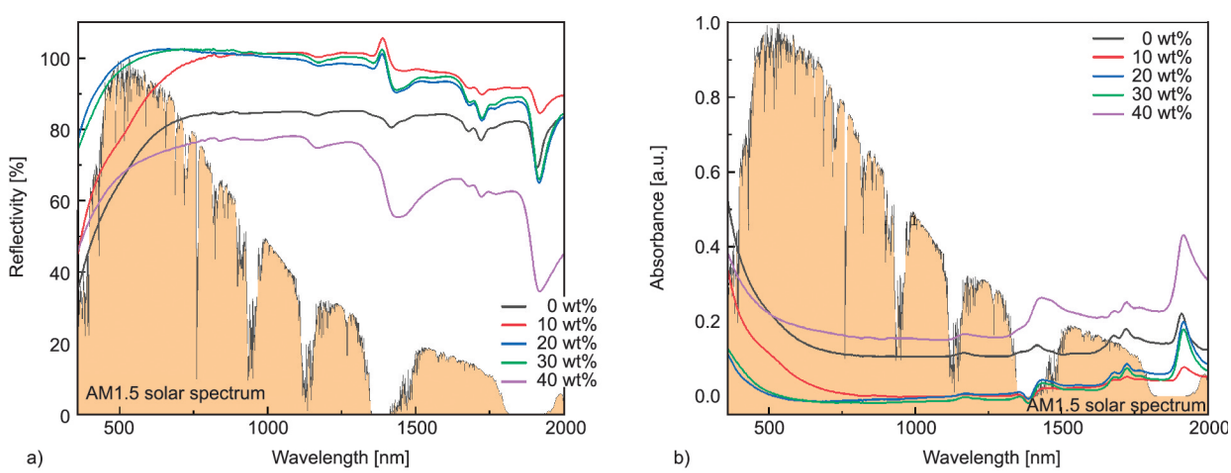

Figure 4. Reflectivity and absorbance of radiative cooling film in the visible and near-infrared wavelength range, (a) is the reflection spectrum of the film in 360–2000 nm, (b) is the absorption spectrum of the film in 360–2000 nm. The normalized AM1.5 solar spectrum is plotted for reference.

decrease is not large in the range of 20–30 wt% content, but the decrease is obvious in the range of 30–40 wt% content. Because the radiative cooling film is made by acetylating lignocellulose microfibrils, the porous structure realizes the reflection of solar radiation, so too many silica microspheres will be blocked in the pores of the microfibrils, making the reflection effect worse. The reason for the negative absorbance and reflectivity greater than 100% in the 750–1250 nm wavelength range is that the reflectivity of the film to light is greater than that of barium sulfate. It can be seen that the addition of silica to the film can increase the reflectivity of the radiative cooling film. This is because silica itself has the ability to resist aging and strongly reflect solar radiation [32]. It can be seen that the reflectivity of each film in the visible wavelength range is very high, and the average reflectivity is 73.05, 86.55, 99.71, 98.44, and 70.33%, the reflectivity of the film with a silica microsphere content of 20 and 30 wt% in the visible wavelength range almost exceeding the normalized solar irradiance. Among them, the highest average reflectance is the film with a silica content of 20 wt%. The reflectivity of the films with 10, 20, and 30 wt% content of silica microspheres in the solar irradiation range is similar, which are 90.95, 86.48, and 87.05%, respectively. However, the reflectivity in the visible light range is quite different, which are 86.55, 99.71, and 98.44%, respectively. At the same time, according to the AM1.5 spectrum, the energy of solar radiation is larger in the visible light range, so when the content of silica microspheres is 20 and 30 wt%, the film can isolate the energy of solar radiation better.

Because the intrinsic absorption of lignocellulose and silica microspheres makes the radiative cooling film strongly absorb (emit) the infrared light in 8–13 μm. The radiative cooling film has extremely low transparency properties, so the infrared transmission spectrum of the film cannot be directly tested. Using Nicolet 6700 infrared spectrometer with an integrating sphere accessory, we can test the reflectivity of the sample film in 2.5–15.5 μm wavelength range. The reflectivity of the films was measured directly using the diffuse reflectance integrating sphere accessory by stacking the gold-coated substrates for baseline scans. At the same time, a gold mirror with a reflectivity of up to 100% is stacked on the back of the test sample, and the infrared rays passing through the sample are reflected back to the integrating sphere accessory so that the reflectivity obtained is the sum of the transmittance and the reflectivity. By obtaining the reflectance spectrum of the sample film, Kirchhoff's law can be used to calculate the infrared emissivity(infrared absorptance) of the sample film to evaluate the infrared radiative capability of the sample film. According to Kirchhoff's law, the ratio of the material's infrared emissivity to the infrared absorptance is 1, so the stronger the material's infrared absorption in the 8–13 μm wavelength range, the stronger the material's infrared emissivity in the 8–13 μm wavelength range. And we can get the infrared emission spectrum of the radiative cooling film in the wavelength range of 7–14 μm through the following relationship, the infrared emission spectrum is shown in Figure 5 (Equation (1)):

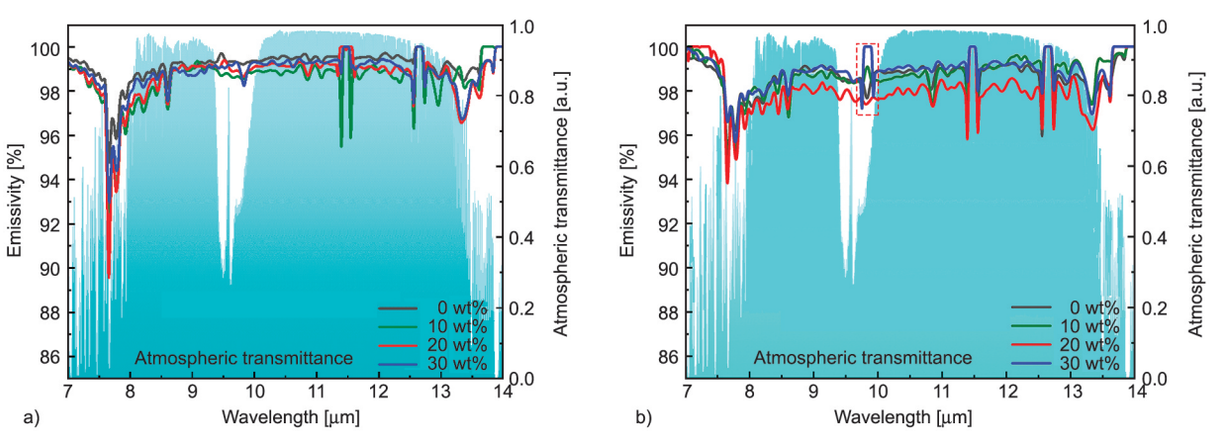

Figure 5. The infrared emissivity of the radiative cooling film in the wavelength range of 7–14 μm. (a) shows the infrared emission spectra at the top of the film in the wavelength range of 7–14 μm. (b) shows the infrared emission spectra at the bottom of the film in the wavelength range of 7–14 μm, where the wavelength range of the marked area is 9.7 μm. The figures are plotted the atmospheric transmittance spectrum under the conditions of AM1.5 and the precipitable amount of 1 mm H_2O as a reference.

$$E(\gamma,\lambda) = A(\gamma,\lambda) = 1 - R(\gamma,\lambda) \quad (1)$$

where $E(\gamma,\lambda)$ [%]: emissivity, $A(\gamma,\lambda)$ [%]: absorptance, $R(\gamma,\lambda)$ [%]: reflectivity, γ is the angle and λ is the wavelength.

Then we quoted the atmospheric transmission spectrum measured by the Gemini Observatory under the conditions of AM1.5 and the precipitable amount of 1 mm H_2O as a reference for the atmospheric window (Lord, S. D., 1992, NASA Technical Memorandum 103957). Because of the characteristics of acetylated lignocellulose, the infrared emissivity of radiative cooling films is generally high. Among them, the infrared emissivity of the top of the film with a silica content of 0–30 wt% is 98.8, 98.4, 98.3, 98.6%, respectively. It can be found that the addition of silica microspheres has almost no effect at the top of the film. However, due to the deposition of silica microspheres at the bottom of the film, the infrared emissivity is significantly increased in the 9.7 μm wavelength range, which is caused by the strong phonon polarization resonances of the silica microspheres in the 9.7 μm wavelength range [24]. When the silica content increases to 30 wt%, the average emissivity of the radiative cooling film is higher, which can reach 98.7%.

X-ray diffraction pattern analysis can further explore the structure and constituents of the radiative cooling film, and through phase analysis, the distribution of silica microspheres on both sides of the film can be obtained. Figure 6 are the XRD pattern of the top and bottom of the radiative cooling film with different content of silica microspheres. It can be found that the XRD patterns of the film with non-silica microspheres are composed of two amorphous peaks centered at 20 and 8°, respectively, and the crystallinity is low. The broad peak centered at 20° is caused by the decrease in crystallinity and the transformation of the structure from a crystalline region to an amorphous region because of the damage of hydrogen bonds in the cellulose network during the acetylation process. This broad peak is the characteristic peak of the amorphous acetyl cellulose [33, 34]. It can be seen from Figure 6a that the addition of silica microspheres reduces the intensity of the characteristic broad peak centered at 20°, while Figure 6b shows that due to the deposition of silica microspheres, the characteristic broad peak centered at 20° of the bottom of the film almost disappeared, which explained the main distribution of silica microspheres and further explained the double-layer structure of the film.

The broad peak centered at 8° is the main feature of semi-crystalline acetyl cellulose, which indicates that the cellulose is disordered during the acetylation process. This disorder is caused by the projection of the substituents along the axis, and the disorder relates to the increase of the distance between the cellulose and the damage of the microfiber structure [35]. It can be found that the XRD pattern at the bottom of the film with 0 wt% silica microspheres has a higher intensity of the broad peak centered at 8° than the top. This is because the bottom of the film is composed of dense acetylated lignocellulose microfibrils, the distance between them decreases, and the diffraction intensity increases. By comparing the relationship between the degree of substitution of acetyl cellulose substituents and the XRD pattern, it

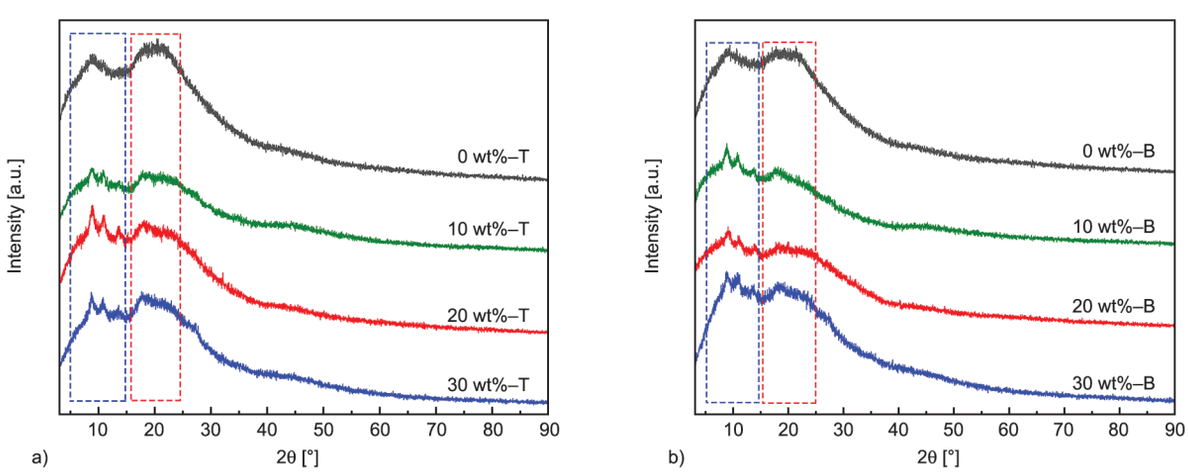

Figure 6. The X-ray diffraction patterns of radiative cooling film with different silica microsphere contents, (a) shows the X-ray diffraction pattern of the top of the film, (b) shows the X-ray diffraction pattern of the bottom of the film.

is found that the crystal form of acetyl cellulose is between cellulose type I and cellulose type II. As the degree of substitution decreases, the crystallinity decreases, and finally, two broad diffraction peaks are formed [36]. This shows that acetylated lignocellulose is mainly composed of acetyl cellulose with a low degree of substitution, and because of its low crystallinity, it is soluble in acetone.

The infrared emissivity characterization of the sample film by infrared spectrometer found that when the silica microsphere content is 30 wt%, because of the resonance of the silica microspheres, the average infrared emissivity of the film is as high as 98.7%, and the average reflectivity and absorbance can reach 98.44% and 0.0029 in the visible wavelength range. In view of the different silica content radiative cooling film, the film with 30 wt% silica content in the film has the best infrared radiation and visible light reflection. For the comparison of radiative cooling performance, the silica microsphere content of 30 wt% is the best, so we choose the acetyl lignocellulose film with a silica content of 30 wt% to compare the radiative cooling performance. The properties of films with different silica microsphere contents are shown in Table 1.

We use a polystyrene circular foam box as the main body of the device to build a radiative cooling test device to test the radiative cooling performance. By digging a cylinder with a diameter of 55 mm and a height of 15 mm on the top of the foam box as the sample chamber for the radiative cooling test, and then place the film in it. The surface of the circular foam box is all covered with aluminum foil, and the high reflectivity of the aluminum foil can prevent direct sunlight from irradiating the test device and affecting the experimental results. In order to ensure that the radiative cooling film is isolated from the external environment, a layer of polyethylene film with an infrared transmittance of up to 90% is laid on the surface of the sample chamber of the radiative cooling performance test device. In addition, the Ethernet type temperature and humidity recorder of Jianda Nishina is used as the temperature recorder. The instrument probe is placed under the radiative cooling film and superimposed the copper sheet of the same material as the probe on the probe to measure the surface temperature of the sample. At the same time, we also prepared radiative cooling materials composed of silica layer and aluminum flakes for comparison, and a blank group is set up in the same way to test the film radiative cooling performance.

In order to accurately test the radiative cooling performance of the film, the test environment selects an outdoor roof with good sunlight conditions and air circulation and chooses a sunny day for the film radiative cooling performance test. The sunrise time is 6:46:47; the sunset time is 18:30:59; the geographic location is 23.039 north latitude and 113.388 east longitude. The weather data on the test day is shown in Table 2 (Data from China Meteorological Administration).

The time period for the night radiative cooling test was from 23:00 to 7:00, and the temperature data was recorded every 1 minute. The time period for the daytime radiative cooling test was from 8:00 to 17:00, the temperature data was recorded every 1 minute. The result is shown in Figure 7.

It can be seen from Figure 7b that the average blank sample temperature is 19.8 °C, the average SiO_2/Al film temperature is 19.1 °C, the average sample temperature is 18.9 °C, and the average temperature difference is 0.9 and 0.2 °C, respectively. Therefore,

Table 2. The weather data on the test day.

Time [hour]	Air pressure [hPa]	Wind direction [°]	Wind speed [m/s]	Relative humidity [%]	Precipitation [mm]
0	1010.6	6	0.6	95	0
3	1010.3	159	3.4	64	0
6	1006.6	199	2.0	59	0
9	1005.1	226	2.1	58	0
12	1006.2	171	3.5	64	0
15	1007.9	320	1.2	89	0

Table 1. Properties of films with different silica microsphere contents.

Silica microsphere content [wt%]	Solar radiation range		'Atmospheric window' range	Visible light range
	Absorbance [a.u.]	Reflectivity [%]	Emissivity [%]	Reflectivity [%]
0	0.172	76.65	98.6	73.05
10	0.038	90.95	98.5	86.55
20	0.025	86.48	98.1	99.71
30	0.017	87.05	98.7	98.44

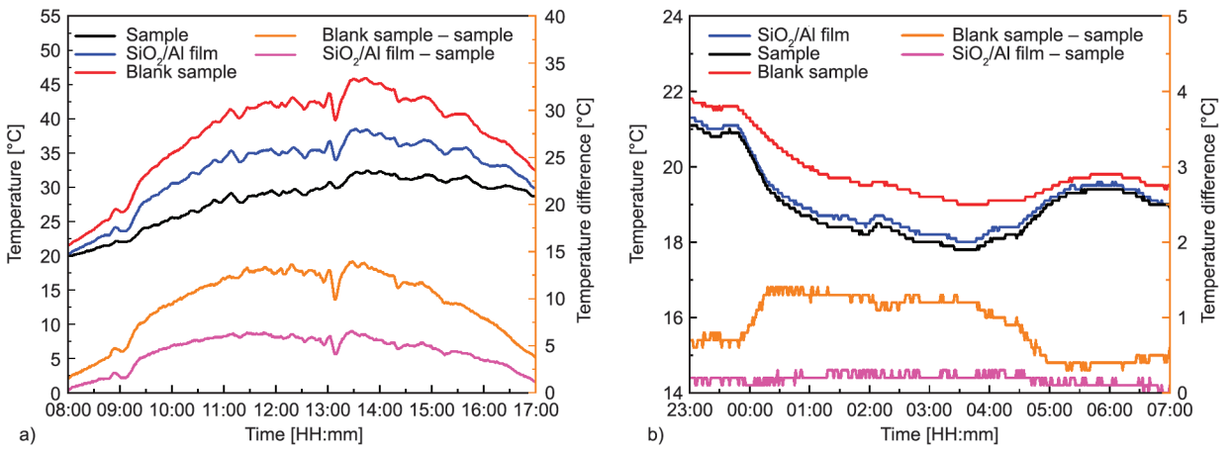

Figure 7. The graph of film's radiative cooling performance, (a) shows the daytime radiative cooling performance of the film, (b) shows the night radiative cooling performance of the film.

the film's night-time radiative cooling energy can be reduced by 0.9 °C compared to the blank sample and reduced by 0.2 °C compared to the SiO_2/Al film. The difference between the blank sample and the sample temperature in the figure is basically stable between 0.3 and 1.4 °C, which shows that the film has great stability in the radiative cooling performance at night, and there is basically no significant change in the radiative cooling performance when the temperature is changing. It can be seen from Figure 7a that the average blank sample temperature is 37.8 °C, the average SiO_2/Al film temperature is 32.6 °C, the average sample temperature is 28.1 °C, and the average temperature difference is 9.6 and 4.4 °C, respectively. Therefore, the daytime radiative cooling energy of the film is lower than the blank sample temperature by 9.6 °C and lower than the SiO_2/Al film temperature by 4.4 °C. The radiative cooling effect of daytime is the result of the film's reflection of sunlight and radiative cooling performance, so the cooling effect is better than that of night radiative cooling. At the same time, in the direct sunlight at noon (12:38:53), the difference between the blank sample temperature and the sample temperature was still 13 °C and reached a maximum value of 13.9 °C at 13:14.The effect of daytime radiative cooling of the film is maintained between 1.6 and 13.9 °C, indicating that the film has excellent daytime radiative cooling performance.

4. Conclusions

We took advantage of the characteristics of wide sources and easy chemical modification of cellulose. Using wood flour as raw material, we use the evaporation deposition technique to prepare a highly spectrally selective dual-layer cellulose-based composite material. The material exhibits minimal absorption and great reflection in the visible light range, and it also exhibits high infrared emission in the 'atmospheric window' range. At the same time, we studied the influence of different silica microsphere content on the material properties. We have found that the addition of silica microspheres can significantly increase the reflectivity of the film. However, when the content of silica microspheres in the film exceeds 10 wt%, the addition in silica content will increase the absorbance and decrease the reflectivity of the film in the wavelength range of 1100–2000 nm. When the content of silica microspheres exceeds 20 wt%, the reflectivity of the film in the wavelength range of 360–1100 nm decreases to varying degrees with the increase of silica microsphere content. Among them, the radiative cooling film with a silica content of 30 wt% exhibits the low absorption of 0.0029 in the visible light range and exhibits the high reflectivity of 98.44% in the 400–800 nm wavelength range. And the film also exhibits high infrared emissivity of 98.7% in the 'atmospheric window' range. In addition, the radiative cooling performance test shows that the film exhibits a cooling of 0.9 °C at night and exhibits a cooling of 9.6 °C under direct sunlight. In addition, by comparing with the SiO_2/Al film, the film exhibits a cooling of 0.2 °C at night and exhibits a cooling of 4.4 °C under direct sunlight. Moreover, the raw material price of the 1 m^2 sample film is only 6 cents. This radiative cooling film outperforms other samples in performance, and the raw material price is far lower than that of other materials. This research work provides a preparation method for daytime radiative cooling materials

with simple technology, cheap raw materials, and wide sources, and also provides a reference for the industrialization of radiative cooling materials and the application of radiative cooling materials in building materials.

Acknowledgements

This work was supported by the Natural Science Foundation of China (51975220 and U1401246), Research Fund for the Doctoral Program of Higher Education of China (20134420120009), Science and Technology Program of Guangdong Province of China (2015A050502047), Science and Technology Program of Guangzhou City of China (201707010367), Dongguan project for introducing innovative scientific research teams (20200607212008) and Training Project of Guangdong Joint Postgraduate Training Demonstration Base. The reference data for this work comes from the National Renewable Energy Laboratory (NREL) and the Gemini Observatory.

References

[1] Yang J., Zhang X., Zhang X., Wang L., Feng W., Li Q.: Beyond the visible: Bioinspired infrared adaptive materials. Advanced Materials, **174**, 2004754 (2021). https://doi.org/10.1002/adma.202004754

[2] Raman A. P., Anoma M. A., Zhu L., Rephaeli E., Fan S.: Passive radiative cooling below ambient air temperature under direct sunlight. Nature, **515**, 540–544 (2014). https://doi.org/10.1038/nature13883

[3] Aili A., Wei Z. Y., Chen Y. Z., Zhao D. L., Yang R. G., Yin X. B.: Selection of polymers with functional groups for daytime radiative cooling. Materials Today Physics, **10**, 100127 (2019). https://doi.org/10.1016/j.mtphys.2019.100127

[4] Gamage S., Kang E. S. H., Åkerlind C., Sardar S., Edberg J., Kariis H., Ederth T., Berggren M., Jonsson M. P.: Transparent nanocellulose metamaterial enables controlled optical diffusion and radiative cooling. Journal of Materials Chemistry C, **8**, 11687–11694 (2020). https://doi.org/10.1039/d0tc01226b

[5] Klemm D., Heublein B., Fink H-P., Bohn A.: Cellulose: Fascinating biopolymer and sustainable raw material. Angewandte Chemie International Edition, **44**, 3358–3393 (2005). https://doi.org/10.1002/anie.200460587

[6] Mohanty A. K., Vivekanandhan S., Pin J-M., Misra M.: Composites from renewable and sustainable resources: Challenges and innovations. Science, **362**, 536–542 (2018). https://doi.org/10.1126/science.aat9072

[7] Zhang H. L., Lin B., Tang J. L., Wang Y. Y., Wang H., Zhang H. L., Cao J. Y., Hou J., Sun M. X., Zhang H. B.: An ethyl cellulose-based supramolecular gel composite coating for metal corrosion protection and its self-healing property from electromagnetic heating effect. Surface and Coatings Technology, **424**, 127647 (2021). https://doi.org/10.1016/j.surfcoat.2021.127647

[8] Kang M., Oderinde O., Han X., Fu G., Zhang Z.: Development of oxidized hydroxyethyl cellulose-based hydrogel enabling unique mechanical, transparent and photochromic properties for contact lenses. International Journal of Biological Macromolecules, **183**, 1162–1173 (2021). https://doi.org/10.1016/j.ijbiomac.2021.05.029

[9] Vasil'kov A., Rubina M., Naumkin A., Buzin M., Dorovatovskii P., Peters G., Zubavichus Y.: Cellulose-based hydrogels and aerogels embedded with silver nanoparticles: Preparation and characterization. Gels, **7**, 82 (2021). https://doi.org/10.3390/gels7030082

[10] Wan Y-L., Hu Y-L., Xu D-X., Huang J-B., Xu F., Wu Y-Y., Zhang X-M.: Fabrication and characterization of cellulose/ lignin microspheres films with UV-blocking (in Chinese). Cailiao Gongcheng-Journal of Materials Engineering, **49**, 56–63 (2021). https://doi.org/10.11868/j.issn.1001-4381.2020.001163

[11] Lai W-F., Yip W., Wong W-T.: UV-shielding and clusteroluminogenic cellulose-based films with tuneable wettability and permeability for dually self-indicating food packaging. Advanced Materials Technologies, **6**, 2100120 (2021). https://doi.org/10.1002/admt.202100120

[12] Zhao B., Hu M., Ao X., Chen N., Pei G.: Radiative cooling: A review of fundamentals, materials, applications, and prospects. Applied Energy, **236**, 489–513 (2019). https://doi.org/10.1016/j.apenergy.2018.12.018

[13] Yin X., Yang R., Tan G., Fan S.: Terrestrial radiative cooling: Using the cold universe as a renewable and sustainable energy source. Science, **370**, 786–791 (2020). https://doi.org/10.1126/science.abb0971

[14] Chen L., Zhang K., Ma M., Tang S., Li F., Niu X.: Sub-ambient radiative cooling and its application in buildings. Building Simulation, **13**, 1165–1189 (2020). https://doi.org/10.1007/s12273-020-0646-x

[15] Li W., Li Y., Shah K.: A materials perspective on radiative cooling structures for buildings. Solar Energy, **207**, 247–269 (2020). https://doi.org/10.1016/j.solener.2020.06.095

[16] Carlosena L., Ruiz-Pardo Á., Feng J., Irulegi O., Hernández-Minguillón R. J., Santamouris M.: On the energy potential of daytime radiative cooling for urban heat island mitigation. Solar Energy, **208**, 430–444 (2020). https://doi.org/10.1016/j.solener.2020.08.015

[17] Suhendri, Hu M., Su Y., Darkwa J., Riffat S.: Implementation of passive radiative cooling technology in buildings: A review. Buildings, **10**, 215 (2020). https://doi.org/10.3390/buildings10120215

[18] Li N., Wang J., Liu D., Huang X., Xu Z., Zhang C., Zhang Z., Zhong M.: Selective spectral optical properties and structure of aluminum phosphate for daytime passive radiative cooling application. Solar Energy Materials and Solar Cells, **194**, 103–110 (2019). https://doi.org/10.1016/j.solmat.2019.01.036

[19] Santamouris M., Feng J.: Recent progress in daytime radiative cooling: Is it the air conditioner of the future? Buildings, **8**, 168 (2018). https://doi.org/10.3390/buildings8120168

[20] Kecebas M. A., Menguc M. P., Kosar A., Sendur K.: Passive radiative cooling design with broadband optical thin-film filters. Journal of Quantitative Spectroscopy and Radiative Transfer, **198**, 179–186 (2017). https://doi.org/10.1016/j.jqsrt.2017.03.046

[21] Ono M., Chen K., Li W., Fan S.: Self-adaptive radiative cooling based on phase change materials. Optics Express, **26**, A777–A787 (2018). https://doi.org/10.1364/oe.26.00a777

[22] Zou C., Ren G., Hossain M. M., Nirantar S., Withayachumnankul W., Ahmed T., Bhaskaran M., Sriram S., Gu M., Fumeaux C.: Metal-loaded dielectric resonator metasurfaces for radiative cooling. Advanced Optical Materials, **5**, 1700460 (2017). https://doi.org/10.1002/adom.201700460

[23] Hossain M. M., Jia B. H., Gu M.: A metamaterial emitter for highly efficient radiative cooling. Advanced Optical Materials, **3**, 1047–1051 (2015). https://doi.org/10.1002/adom.201500119

[24] Zhai Y., Ma Y., David S. N., Zhao D., Lou R., Tan G., Yang R., Yin X.: Scalable-manufactured randomized glass-polymer hybrid metamaterial for daytime radiative cooling. Science, **355**, 1062–1066 (2017). https://doi.org/10.1126/science.aai7899

[25] Zhao D., Aili A., Zhai Y., Lu J., Kidd D., Tan G., Yin X., Yang R.: Subambient cooling of water: Toward real-world applications of daytime radiative cooling. Joule, **3**, 111–123 (2019). https://doi.org/10.1016/j.joule.2018.10.006

[26] Atiganyanun S., Plumley J. B., Han S. J., Hsu K., Cytrynbaum J., Peng T. L., Han S. M., Han S. E.: Effective radiative cooling by paint-format microsphere-based photonic random media. ACS Photonics, **5**, 1181–1187 (2018). https://doi.org/10.1021/acsphotonics.7b01492

[27] Mandal J., Fu Y., Overvig A. C., Jia M., Sun K., Shi N. N., Zhou H., Xiao X., Yu N., Yang Y.: Hierarchically porous polymer coatings for highly efficient passive daytime radiative cooling. Science, **362**, 315–319 (2018). https://doi.org/10.1126/science.aat9513

[28] Xiang B., Zhang R., Luo Y., Zhang S., Xu L., Min H., Tang S., Meng X.: 3D porous polymer film with designed pore architecture and auto-deposited SiO_2 for highly efficient passive radiative cooling. Nano Energy, **81**, 105600 (2021). https://doi.org/10.1016/j.nanoen.2020.105600

[29] Li T., Zhai Y., He S., Gan W., Wei Z., Heidarinejad M., Dalgo D., Mi R., Zhao X., Song J., Dai J., Chen C., Aili A., Vellore A., Martini A., Yang R., Srebric J., Yin X., Hu L.: A radiative cooling structural material. Science, **364**, 760–763 (2019). https://doi.org/10.1126/science.aau9101

[30] Musa S., Richter O., Balsam M., Kneer A., Barbe S.: Macroporous films from acetylated lignin and cellulose as precursors for smart coatings based on regenerated wood. European Journal of Wood and Wood Products, **76**, 1363–1366 (2018). https://doi.org/10.1007/s00107-018-1308-x

[31] Liu J., He G., Lu N., Li J.: Fabrication of photo-absorption enhanced black TiO_2-SiO_2 by flame spraying. Materials Research Express, **4**, 125503 (2017). https://doi.org/10.1088/2053-1591/aa9e21

[32] Wang Y. Z., Li Y., Jia W. N., Yue C., Ma D.: Study on anti-aging performance of composite materials of PP-G-an/Pp/SiO_2. Advanced Materials Research, **634–638**, 2023–2027 (2012). https://doi.org/10.4028/www.scientific.net/AMR.634-638.2023

[33] Fan X., Liu Z-W., Lu J., Liu Z-T.: Cellulose triacetate optical film preparation from ramie fiber. Industrial and Engineering Chemistry Research, **48**, 6212–6215 (2009). https://doi.org/10.1021/ie801703x

[34] Filho G. R., da Cruz S. F., Pasquini D., Cerqueira D. A., da Souza Prado V., de Assuncao R. M. N.: Water flux through cellulose triacetate films produced from heterogeneous acetylation of sugar cane bagasse. Journal of Membrane Science, **177**, 225–231 (2000). https://doi.org/10.1016/s0376-7388(00)00469-5

[35] Barud H. S., de Araujo Júnior A. M., Santos D. B., de Assuncao R. M. N., Meireles C. S., Cerqueira D. A., Filho G. R., Ribeiro C. A., Messaddeq Y., Ribeiro S. J. L.: Thermal behavior of cellulose acetate produced from homogeneous acetylation of bacterial cellulose. Thermochimica Acta, **471**, 61–69 (2008). https://doi.org/10.1016/j.tca.2008.02.009

[36] Daud W. R. W., Djuned F. M.: Cellulose acetate from oil palm empty fruit bunch via a one step heterogeneous acetylation. Carbohydrate Polymers, **132**, 252–260 (2015). https://doi.org/10.1016/j.carbpol.2015.06.011